

## Climatic modulation of recent trends in ocean acidification in the California Current System

This content has been downloaded from IOPscience. Please scroll down to see the full text.

2016 Environ. Res. Lett. 11 014007

(<http://iopscience.iop.org/1748-9326/11/1/014007>)

View [the table of contents for this issue](#), or go to the [journal homepage](#) for more

Download details:

IP Address: 210.77.64.106

This content was downloaded on 30/03/2017 at 11:55

Please note that [terms and conditions apply](#).

You may also be interested in:

[Sensitivity of ocean acidification and oxygen to the uncertainty in climate change](#)

Long Cao, Shuangjing Wang, Meidi Zheng et al.

[Response of ocean acidification to a gradual increase and decrease of atmospheric CO<sub>2</sub>](#)

Long Cao, Han Zhang, Meidi Zheng et al.

[Could artificial ocean alkalization protect tropical coral ecosystems from ocean acidification?](#)

Ellias Y Feng (), David P Keller, Wolfgang Koeve et al.

[Presence of nitrous oxide hotspots in the coastal upwelling area off central Chile: an analysis of temporal variability based on ten years of a biogeochemical time series](#)

L Farías, V Besoain and S García-Loyola

[Simulated reduction in upwelling of tropical oxygen minimum waters in a warmer climate](#)

M S Glessmer, W Park and A Oschlies

[The role of open ocean boundary forcing on seasonal to decadal-scale variability and long-term change of natural shelf hypoxia](#)

Pedro M S Monteiro, Boris Dewitte, Mary I Scranton et al.

[Observed southern upper-ocean warming over 2005–2014 and associated mechanisms](#)

William Llovel and Laurent Terray

[Anticipating ocean acidification's economic consequences for commercial fisheries](#)

Sarah R Cooley and Scott C Doney

[Is anthropogenic sea level fingerprint already detectable in the Pacific Ocean?](#)

H Palanisamy, B Meyssignac, A Cazenave et al.

## Environmental Research Letters



## LETTER

## Climatic modulation of recent trends in ocean acidification in the California Current System

## OPEN ACCESS

RECEIVED  
18 July 2015REVISED  
21 December 2015ACCEPTED FOR PUBLICATION  
22 December 2015PUBLISHED  
19 January 2016

Original content from this work may be used under the terms of the [Creative Commons Attribution 3.0 licence](#).

Any further distribution of this work must maintain attribution to the author(s) and the title of the work, journal citation and DOI.

G Turi<sup>1</sup>, Z Lachkar<sup>2</sup>, N Gruber and M Münnich

Environmental Physics, Institute of Biogeochemistry and Pollutant Dynamics, ETH Zürich, Zürich, Switzerland

<sup>1</sup> Present address: CIRES, University of Colorado at Boulder, and NOAA/ESRL, Boulder, Colorado, USA.<sup>2</sup> Present address: Center for Prototype Climate Modeling, New York University, Abu Dhabi, UAE.E-mail: [giuliana.turi@env.ethz.ch](mailto:giuliana.turi@env.ethz.ch)**Keywords:** California Current System, ocean acidification, coastal ocean modeling, hindcast simulation**Abstract**

We reconstruct the evolution of ocean acidification in the California Current System (CalCS) from 1979 through 2012 using hindcast simulations with an eddy-resolving ocean biogeochemical model forced with observation-based variations of wind and fluxes of heat and freshwater. We find that domain-wide pH and  $\Omega_{\text{arag}}$  in the top 60 m of the water column decreased significantly over these three decades by about  $-0.02 \text{ decade}^{-1}$  and  $-0.12 \text{ decade}^{-1}$ , respectively. In the nearshore areas of northern California and Oregon, ocean acidification is reconstructed to have progressed much more rapidly, with rates up to 30% higher than the domain-wide trends. Furthermore, ocean acidification penetrated substantially into the thermocline, causing a significant domain-wide shoaling of the aragonite saturation depth of on average  $-33 \text{ m decade}^{-1}$  and up to  $-50 \text{ m decade}^{-1}$  in the nearshore area of northern California. This resulted in a coast-wide increase in nearly undersaturated waters and the appearance of waters with  $\Omega_{\text{arag}} < 1$ , leading to a substantial reduction of habitat suitability. Averaged over the whole domain, the main driver of these trends is the oceanic uptake of anthropogenic  $\text{CO}_2$  from the atmosphere. However, recent changes in the climatic forcing have substantially modulated these trends regionally. This is particularly evident in the nearshore regions, where the total trends in pH are up to 50% larger and trends in  $\Omega_{\text{arag}}$  and in the aragonite saturation depth are even twice to three times larger than the purely atmospheric  $\text{CO}_2$ -driven trends. This modulation in the nearshore regions is a result of the recent marked increase in alongshore wind stress, which brought elevated levels of dissolved inorganic carbon to the surface via upwelling. Our results demonstrate that changes in the climatic forcing need to be taken into consideration in future projections of the progression of ocean acidification in coastal upwelling regions.

**1. Introduction**

The primary driver for the large-scale acidification of the world's oceans is the increase in anthropogenic  $\text{CO}_2$  in the atmosphere, caused by the burning of fossil fuels and land use change (e.g., Orr *et al* 2005, Doney *et al* 2009, Rhein *et al* 2013). The resulting disequilibrium in  $\text{CO}_2$  across the air–sea interface forces anthropogenic  $\text{CO}_2$  into the ocean, causing a global increase in the dissolved  $\text{CO}_2$  concentration, and also a decrease in pH and in the saturation state,  $\Omega$ , with regard to calcium carbonate ( $\text{CaCO}_3$ ) minerals (e.g., Feely *et al* 2004, Orr *et al* 2005, Zeebe 2012). Yet, it is

well recognized that local changes in ocean circulation and ocean biology, or other processes, such as river input (e.g., Cai *et al* 2011, Breitburg *et al* 2015) or atmospheric deposition (e.g., Doney *et al* 2007) can substantially modulate the evolution of oceanic pH and  $\Omega$ . Especially in coastal systems ocean acidification may progress rather differently than in the open ocean. This is due in part to their proximity to land (e.g., Duarte *et al* 2013) but also owing to the high potential in coastal systems for local changes in circulation and biology to impact the ocean's carbonate system (e.g., Turi *et al* 2014). Eastern boundary upwelling systems (EBUS) may be particularly prone

to such modifications of atmospheric CO<sub>2</sub>-driven ocean acidification, because of the key role of the coastal upwelling process, which makes these systems naturally low in pH and  $\Omega$ . Thus, relatively small changes in the intensity of upwelling in these systems may cause substantial changes in the rate of progression of ocean acidification (e.g., Feely *et al* 2008, Hauri *et al* 2009, Gruber 2011, Hofmann *et al* 2011, Gruber *et al* 2012, Alin *et al* 2012, Harris *et al* 2013, Rhein *et al* 2013, Bates *et al* 2014, Lachkar 2014, Williams *et al* 2015).

Recent studies suggest that alongshore, upwelling-favorable wind stress has increased in nearly all of the EBUS (Sydeman *et al* 2014), including the California Current System (CalCS; e.g., Bakun 1990, Schwing and Mendelssohn 1997, Mendelssohn and Schwing 2002, Demarcq 2009, García-Reyes and Largier 2010, Narayan *et al* 2010, Seo *et al* 2012). This is consistent with the hypothesis by Bakun (1990) that the strengthening of the thermal land–sea gradient driven by global surface warming will cause stronger equatorward winds along the western coasts of the continents. This hypothesis also implies that the intensification of upwelling may persist as the planet continues to warm (e.g., Snyder *et al* 2003, Diffenbaugh *et al* 2004, Wang *et al* 2015).

So far, any relevant observations of ocean acidification parameters in EBUS are primarily limited to the 21st century (Borges *et al* 2009), which makes it challenging to investigate how these changes in upwelling-favorable winds might have altered the progression of ocean acidification over decadal time scales. In fact, the degree to which EBUS, and particularly the CalCS, are prone to ocean acidification has emerged clearly only in the last decade (e.g., Feely *et al* 2008, 2009, Wootton *et al* 2008, Hauri *et al* 2009, Gruber *et al* 2012, Hauri *et al* 2013a, 2013b, Leinweber and Gruber 2013, Bednaršek *et al* 2014). For instance, Feely *et al* (2008) observed waters undersaturated with respect to aragonite, the least stable mineral form of CaCO<sub>3</sub>, within the top 20–40 m of the water column in some CalCS coastal regions. Bednaršek *et al* (2014) reported that within the top 100 m up to 70%–90% of the total water volume was undersaturated in widespread areas along the coast, causing measurable shell dissolution in the pteropod *Limacina helicina*. Although coastal upwelling regions such as the CalCS tend to be accustomed to extreme fluctuations in pH and  $\Omega$  due to the seasonality and episodicity of wind-driven upwelling (e.g., Hauri *et al* 2009, Juranek *et al* 2009, Hofmann *et al* 2011, Frieder *et al* 2012, Harris *et al* 2013, Leinweber and Gruber 2013), it is very likely that these regions will become exposed to more frequent, prolonged and intense events of this nature in the near future (Gruber *et al* 2012, Hauri *et al* 2013a, 2013b). Moreover, an acceleration of ocean acidification reduces the time that calcifying organisms have to adapt to such changes and can therefore pose an increased risk to local ecosystem

services (e.g., Soto 2002, Barton *et al* 2012, 2015, Waldbusser *et al* 2014, 2015, Waldbusser and Salisbury 2014, Bednaršek and Ohman 2015).

Given the lack of long-term observations documenting the progression of ocean acidification over the last few decades, hindcast model simulations forced with observation-based estimates of variations in winds and the fluxes of heat and freshwater are one of the few means to reconstruct this history (see, e.g., Lenton *et al* (2015), for an empirical model-based approach). We follow this model-based approach and employ a coupled physical-biogeochemical model on the basis of the Regional Oceanic Modeling System (ROMS), configured for the CalCS at eddy-permitting resolution. Our objectives are (i) to investigate the progression of ocean acidification in the CalCS over the period from 1979 to 2012, i.e., over the period when atmospheric CO<sub>2</sub> increased from about 335  $\mu\text{atm}$  to 394  $\mu\text{atm}$ , and (ii) to separate the effect of the rise in atmospheric CO<sub>2</sub> from the effect of changes in the climatic forcing. We do not take into consideration other processes that potentially affect ocean acidification, such as changes in deposition by rivers and through the atmosphere, as we assume these effects to be of minor importance in this region.

## 2. Model and methods

We use an eddy-resolving coupled physical-biogeochemical ocean model to simulate the evolution of ocean acidification in the CalCS from 1979 to 2012. The physical model is based on the UCLA-ETH version of ROMS (Marchesiello *et al* 2003, Shchepetkin and McWilliams 2005). Coupled to the physical model is a nitrogen-based nutrient-phytoplankton-zooplankton-detritus model (Gruber *et al* 2006) that was extended with a carbon module (Gruber *et al* 2012, Hauri *et al* 2013b, Turi *et al* 2014). The CalCS model setup employed here has a resolution of 5 km, and extends roughly from 30°N to 50°N along the US West Coast and about 1250 km westward into the open Pacific. This grid setup and these parameters correspond exactly to those used by Turi *et al* (2014). While previous simulations with similar setups using ROMS were climatologically forced (Gruber 2011, Hauri *et al* 2013b, Turi *et al* 2014), we focus here on the impact of variations and trends in the atmospheric forcing.

We ran two hindcast simulations (‘HCast’) with variable atmospheric forcing and lateral boundary conditions, with the two runs differing only in the applied wind stress forcing and their length of simulation. For both HCast simulations, we used daily fluxes of heat and freshwater from ECMWF’s ERA-Interim reanalysis (Dee *et al* 2011). Atmospheric CO<sub>2</sub> was prescribed to follow the observed atmospheric trend (Cooperative Global Atmospheric Data Integration Project 2013). We forced the model at the lateral

boundaries with a combination of climatological fields based on observations and time-varying anomaly fields derived from a global hindcast simulation with the NCAR CCSM3 model (Graven *et al* 2012).

In the first hindcast simulation ('HCast-ERA1'), we used the daily wind stress forcing from ERA-Interim as well. However, as ERA-Interim has a relatively coarse resolution of  $\sim 79$  km, we ran a second hindcast simulation ('HCast-CCMP') where we forced the model with daily wind stress computed from the wind speed data of NASA's CCMP reanalysis dataset (Atlas *et al* 2011). This latter forcing has a horizontal resolution of  $0.25^\circ$ , and therefore may be better suited to capture the response of coastal upwelling to recent climate change (e.g., Jacox *et al* 2014, Renault *et al* 2015). As CCMP provides only wind speed, we calculated wind stress using the drag coefficient formulation after Hersbach (2011). Due to differing data availability, the HCast-ERA1 simulation was run for the entire analysis period, i.e., 1979–2012, whereas the HCast-CCMP simulation only spans the period from 1988 to 2011.

For both HCast simulations, the model was spun up for 10 years starting from observations and using so-called 'normal-year forcing', i.e., climatological monthly forcing with added daily variations from a particular year. The spinup for the HCast-ERA1 simulation used the normal-year forcing from ERA-interim and began in the year 1969 with daily anomalies from 1985, while the spinup for the HCast-CCMP simulation was initialized in 1978 and was forced with the normal year forcing from CCMP from 1991. More details on the model's atmospheric forcing and the lateral boundary conditions are given in the appendix.

The appendix also contains a detailed model assessment section, in which we demonstrate that both forcing products are able to reproduce the observed cooling over the last few decades (e.g., García-Reyes and Largier 2010, Seo *et al* 2012), as well as the accompanying increase in near-surface chlorophyll since the late 1990s (e.g., Kahru *et al* 2009, 2012). In addition, this setup, forced with a different set of atmospheric boundary conditions than used previously, performs on average as well as previous setups with regard to long-term mean sea surface temperature (SST) and chlorophyll (not shown; Gruber 2011, Hauri *et al* 2013b, Turi *et al* 2014). The two forcing products have complimentary strengths and weaknesses, with HCast-CCMP better capturing the trends in SST, while HCast-ERA1 is better in simulating the alongshore increase in chlorophyll.

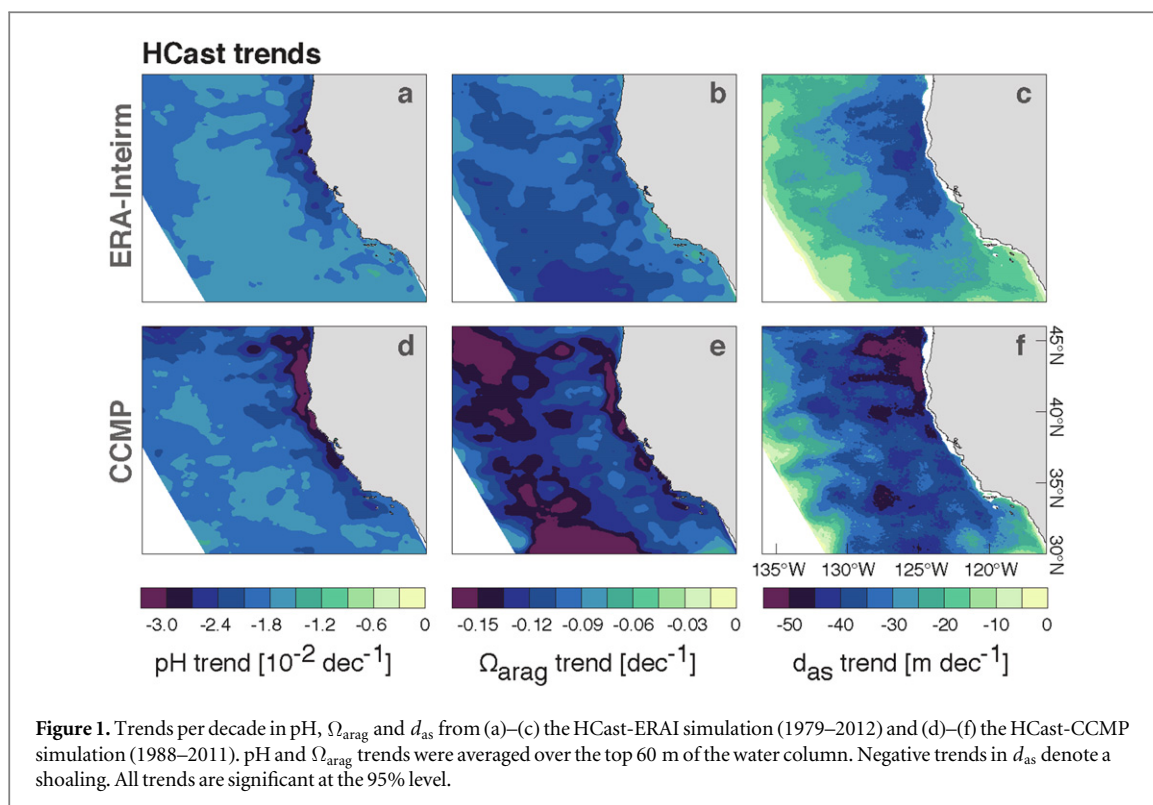
To separate out the effect of recent changes in the climatic forcing on ocean acidification, we additionally ran two 'constant climate' ('CCLim') simulations under both forcing products ('CCLim-ERA1' and 'CCLim-CCMP'). In these simulations, only atmospheric  $\text{CO}_2$  and lateral dissolved inorganic carbon (DIC) were allowed to increase, while the other surface and lateral boundary conditions are climatological

reflecting a normal year, i.e., the same boundary conditions we had used for the spinup. Assuming that the trends from the HCast and CCLim simulations are linearly additive, we use the difference between these two simulations to identify the contribution of variable climatic forcing, without the effect of increasing atmospheric  $\text{CO}_2$  (i.e., HCast-CCLim). We decided to use this approach of linear partitioning instead of directly computing trends from a 'climate only' simulation in order to remove any model internal variability that is unrelated to changes in the climatic forcing. By comparing our trend results to trends from the 'climate-only' simulation and finding only minimal differences in absolute trend values and domain-wide patterns, we determined that in our case this approach is valid (not shown).

The full suite of carbonate chemistry parameters was calculated offline from the modeled state variables temperature, salinity, nitrate, DIC and alkalinity (Alk) using the carbonate chemistry routines from the ocean carbon-cycle model intercomparison project (Orr *et al* 2000). We calculate all trends by least squares linear regressions, using the  $p$ -value from a Student's  $t$ -test for the statistical significance, accounting for autocorrelation by reducing the degrees of freedom according to the equivalent sample size (after Zwiers and von Storch 1995).

### 3. Evolution of ocean acidification

Over the whole model domain and over the period 1979/1988 to 2012, we model in the HCast simulations a decrease in surface pH and  $\Omega_{\text{arag}}$  in the top 60 m of the water column of  $-0.020 \pm 0.002 \text{ dec}^{-1}$  and  $-0.12 \pm 0.02 \text{ dec}^{-1}$ , respectively (averaged over both HCast simulations with the uncertainty representing the spatial variability; figures 1(a), (b), (d) and (e) and table 1). These CalCS domain-wide trends in ocean acidification correspond roughly to those observed globally and in particular for the North Pacific (see table 6 in Williams *et al* 2015). Lauvset *et al* (2015) estimated a global surface pH trend of  $-0.018 \pm 0.004 \text{ dec}^{-1}$  for the period 1991–2011, which is statistically indistinguishable from our result for the whole CalCS domain (table 1). In particular, for the Hawaii Ocean Time (HOT) series at Station ALOHA and for the time period 1988–2014, Bates *et al* (2014) found decreases in pH and  $\Omega_{\text{arag}}$  of  $-0.016 \pm 0.001 \text{ dec}^{-1}$  and  $-0.084 \pm 0.011 \text{ dec}^{-1}$ , respectively. The IPCC's Fifth Assessment Report (Rhein *et al* 2013) confirms these trends for HOT and offers a further estimate for the pH decline in the North Pacific of  $-0.017 \text{ dec}^{-1}$ , based on two hydrographic lines along  $152^\circ\text{W}$  in 1991 and 2006 (Byrne *et al* 2010). Furthermore, Fay and McKinley (2013) established that surface ocean  $p\text{CO}_2$  trends in the north Pacific from 1981 to 2010 were comparable to the increase in atmospheric  $p\text{CO}_2$  over the same time



period (roughly  $17 \mu\text{atm dec}^{-1}$ ; black line in figure 2(b)). This trend is very close to our modeled  $p\text{CO}_2$  trend for the CalCS of  $18.8 \pm 3.5 \mu\text{atm dec}^{-1}$  (table 1).

The ocean acidification signal penetrates deeply into the thermocline of the CalCS, causing a significant domain-wide shoaling of the aragonite saturation depth ( $d_{\text{as}}$ ; i.e., the depth below which  $\Omega_{\text{arag}} < 1$ ) by an average rate of  $-33 \pm 6 \text{ m dec}^{-1}$  (figures 1(c) and (f)). The strongest upward migration of  $d_{\text{as}}$  occurred in the northern nearshore regions around Cape Mendocino ( $\sim 40^\circ\text{N}$ ), with regional values of more than  $50 \text{ m dec}^{-1}$ . This result is comparable to the  $d_{\text{as}}$  trend of  $50 \text{ m dec}^{-1}$  inferred by Feely *et al* (2012) from two repeat hydrography sections measured in 1994 and 2004 along a transect line crossing through the CalCS. These changes occur at a mean depth of around  $-200 \text{ m}$  in the model, which is somewhat shallower than the observed depth (Feely *et al* 2008, Gruber *et al* 2012). Nonetheless, both modeled and measured results indicate that this shoaling is likely responsible for the substantial compression of habitat suitability for organisms sensitive to ocean acidification across the entire CalCS (e.g., Feely *et al* 2008, Bednaršek *et al* 2014, Bednaršek and Ohman 2015).

Substantial regional differences exist in the trends across the CalCS. In particular, we find much stronger trends in the nearshore areas, although to different degrees in the two simulations. In the HCast-ERA-Interim simulation, the region of largest trends is located between San Francisco Bay, California, and Cape Blanco, Oregon ( $\sim 38\text{--}43^\circ\text{N}$ ; figures 1(a)–(c)), whereas

in the HCast-CCMP simulation, the region of strongest increase extends further to the north and to the south ( $\sim 35\text{--}45^\circ\text{N}$ ; figures 1(d)–(f); see figure 2(a) for geographical locations). In these areas, we have reconstructed maximum decreases in pH and  $\Omega_{\text{arag}}$  of up to  $-0.03 \text{ dec}^{-1}$  and  $-0.15 \text{ dec}^{-1}$ , respectively, and a maximum shoaling of  $d_{\text{as}}$  of up to  $-50 \text{ m dec}^{-1}$ . In contrast to the trends in pH, which show a strong cross-shore gradient, the regions of strongest trends in  $\Omega_{\text{arag}}$  and  $d_{\text{as}}$  extend up to 500–600 km offshore.

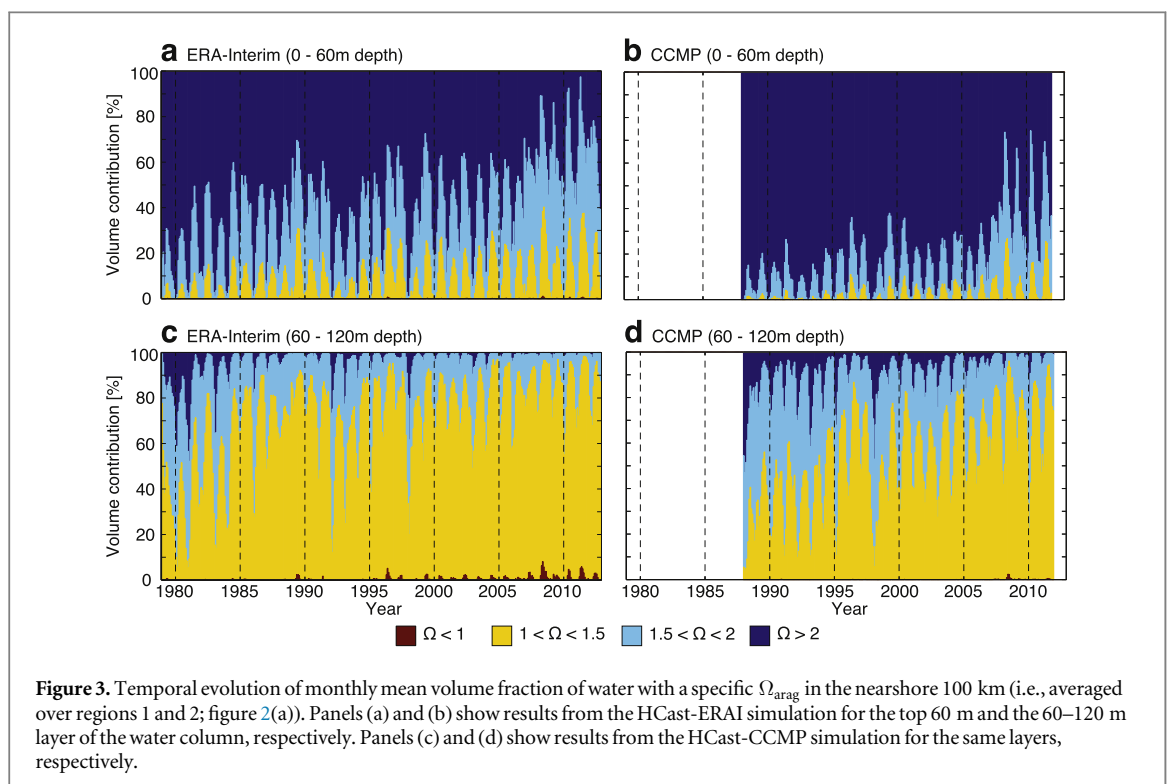
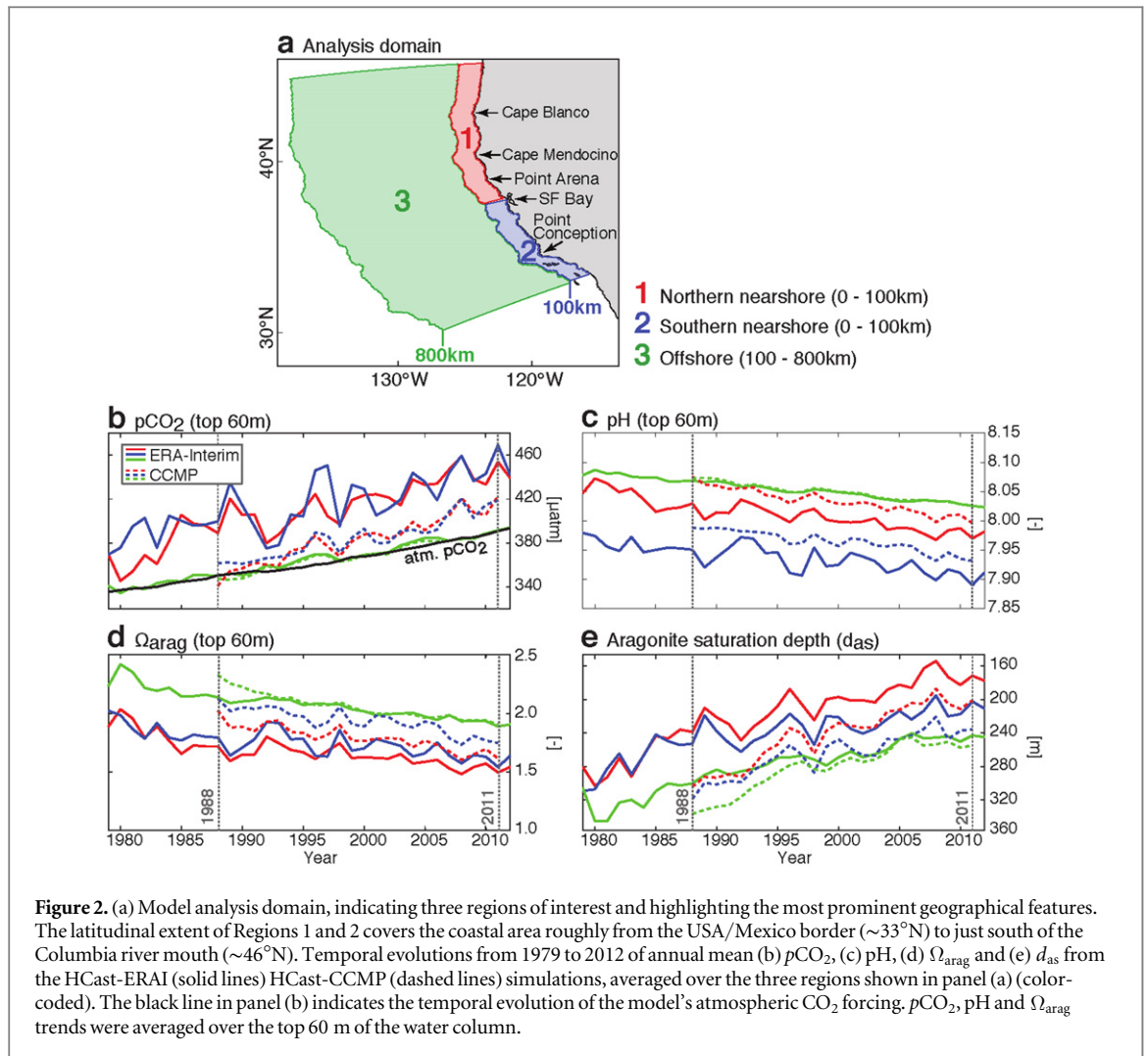
To quantify these trends in more detail, we focus our analysis on three regions within our model domain (figure 2(a)). In both HCast simulations, the largest trends occur in the northern coastal region (R1), where  $p\text{CO}_2$  trends are on average  $5 \mu\text{atm dec}^{-1}$  larger than in the southern coastal region (R2; figure 2(b)). Similarly, pH and  $\Omega_{\text{arag}}$  decrease by about  $-0.005 \text{ dec}^{-1}$  and  $-0.01 \text{ dec}^{-1}$  more, and  $d_{\text{as}}$  shoals by about  $-13 \text{ m dec}^{-1}$  more in R1 compared to R2 (figures 2(c)–(e)). Trends in the offshore region (R3) are the smallest for all three variables in both HCast simulations.

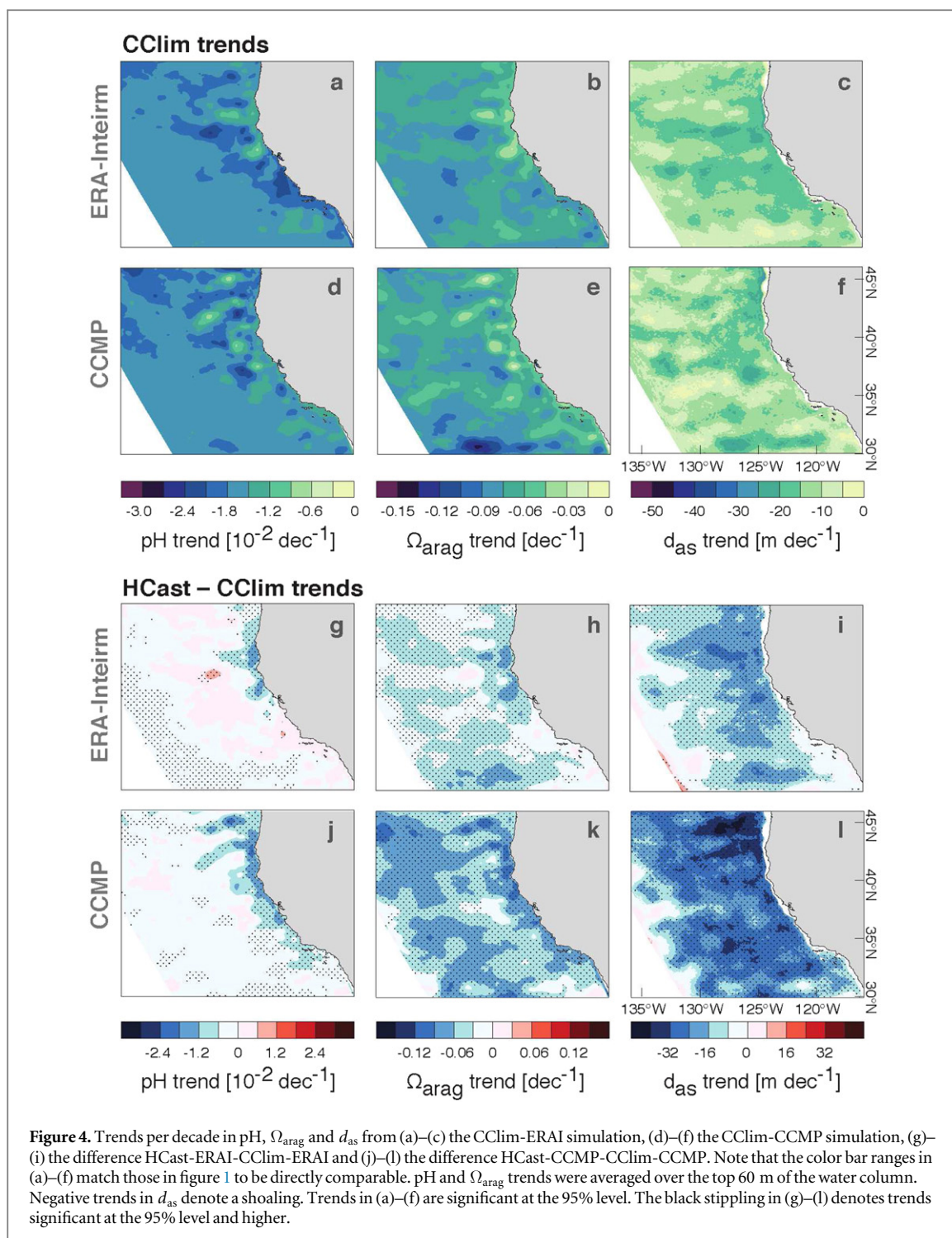
The HCast-CCMP simulation consistently exhibits larger domain-wide and regional trends in  $p\text{CO}_2$ , pH,  $\Omega_{\text{arag}}$  and  $d_{\text{as}}$  than the HCast-ERA-Interim simulation (table 1). This can partly be explained by the larger alongshore wind stress trends in CCMP compared to ERA-Interim (figure 6(c)), especially in the nearshore 100 km. This could have a more offshore-reaching effect on ocean acidification due to the anomalous upwelling and subsequent offshore transport of waters high in DIC and low in pH and carbonate ion

**Table 1.** Trends per decade in  $p\text{CO}_2$ , pH,  $\Omega_{\text{arag}}$  and  $d_{\text{as}}$  from the HCast and CCLim simulations under ERA-Interim and under CCMP forcing. The ‘climatic modulation’ is defined as (HCast-CCLim)/CCLim. Trends were averaged over the whole model analysis domain (‘total’; sum of R1–R3; figure 2(a)) and over the three regions R1–R3 separately and are all significant at the 95% level. Negative trends in  $d_{\text{as}}$  denote a shoaling.  $p\text{CO}_2$ , pH,  $\Omega_{\text{arag}}$  were averaged over the top 60 m of the water column. The uncertainty in the trends represents the spatial variability, i.e., standard deviation, over the respective regions.

Variable	Region <sup>a</sup>	ERA-Interim			CCMP		
		HCast	CCLim	Climatic modulation (%)	HCast	CCLim	Climatic modulation (%)
$p\text{CO}_2$ ( $\mu\text{atm dec}^{-1}$ )	Total	17.9 ± 3.1	17.7 ± 2.9	1.1	19.6 ± 3.9	17.1 ± 2.0	14.6
	R1	25.8 ± 3.6	17.9 ± 3.5	44.1	28.9 ± 3.3	18.4 ± 2.2	57.1
	R2	20.6 ± 2.7	25.5 ± 2.6	−19.2	24.2 ± 2.9	17.6 ± 1.8	37.5
	R3	17.0 ± 1.8	17.2 ± 2.1	−1.2	18.5 ± 2.3	17.0 ± 2.0	8.8
	Total	−0.018 ± 0.002	−0.017 ± 0.002	5.9	−0.021 ± 0.003	−0.017 ± 0.002	23.5
pH ( $\text{dec}^{-1}$ )	R1	−0.024 ± 0.002	−0.016 ± 0.002	50.0	−0.029 ± 0.003	−0.017 ± 0.002	70.6
	R2	−0.019 ± 0.002	−0.020 ± 0.002	−5.0	−0.024 ± 0.003	−0.016 ± 0.002	50.0
	R3	−0.018 ± 0.001	−0.017 ± 0.002	5.9	−0.020 ± 0.002	−0.017 ± 0.002	17.6
	Total	−0.11 ± 0.01	−0.07 ± 0.01	45.8	−0.13 ± 0.02	−0.07 ± 0.01	87.1
	R1	−0.11 ± 0.01	−0.06 ± 0.01	91.1	−0.14 ± 0.02	−0.06 ± 0.01	130.5
$1 \text{ cm } \Omega_{\text{arag}}$ ( $\text{dec}^{-1}$ )	R2	−0.09 ± 0.01	−0.07 ± 0.01	19.2	−0.13 ± 0.01	−0.06 ± 0.01	120.3
	R3	−0.11 ± 0.01	−0.07 ± 0.01	45.2	−0.13 ± 0.02	−0.07 ± 0.01	84.5
	Total	−28.4 ± 6.1	−14.3 ± 3.4	98.6	−38.2 ± 6.5	−12.7 ± 3.9	200.8
	R1	−36.3 ± 3.4	−16.6 ± 3.7	118.7	−46.6 ± 4.5	−15.9 ± 4.4	193.1
	R2	−23.5 ± 6.0	−15.7 ± 2.7	49.7	−33.7 ± 6.7	−11.1 ± 2.2	203.6
$d_{\text{as}}$ ( $\text{m dec}^{-1}$ )	R3	−28.1 ± 5.8	−14.1 ± 3.3	99.3	−37.8 ± 6.1	−12.5 ± 3.8	202.4

<sup>a</sup> The surface areas of R1–R3 are 98 650 km<sup>2</sup>, 69 785 km<sup>2</sup> and 1313 341 km<sup>2</sup>, respectively. The total surface area amounts to 1481 776 km<sup>2</sup>.



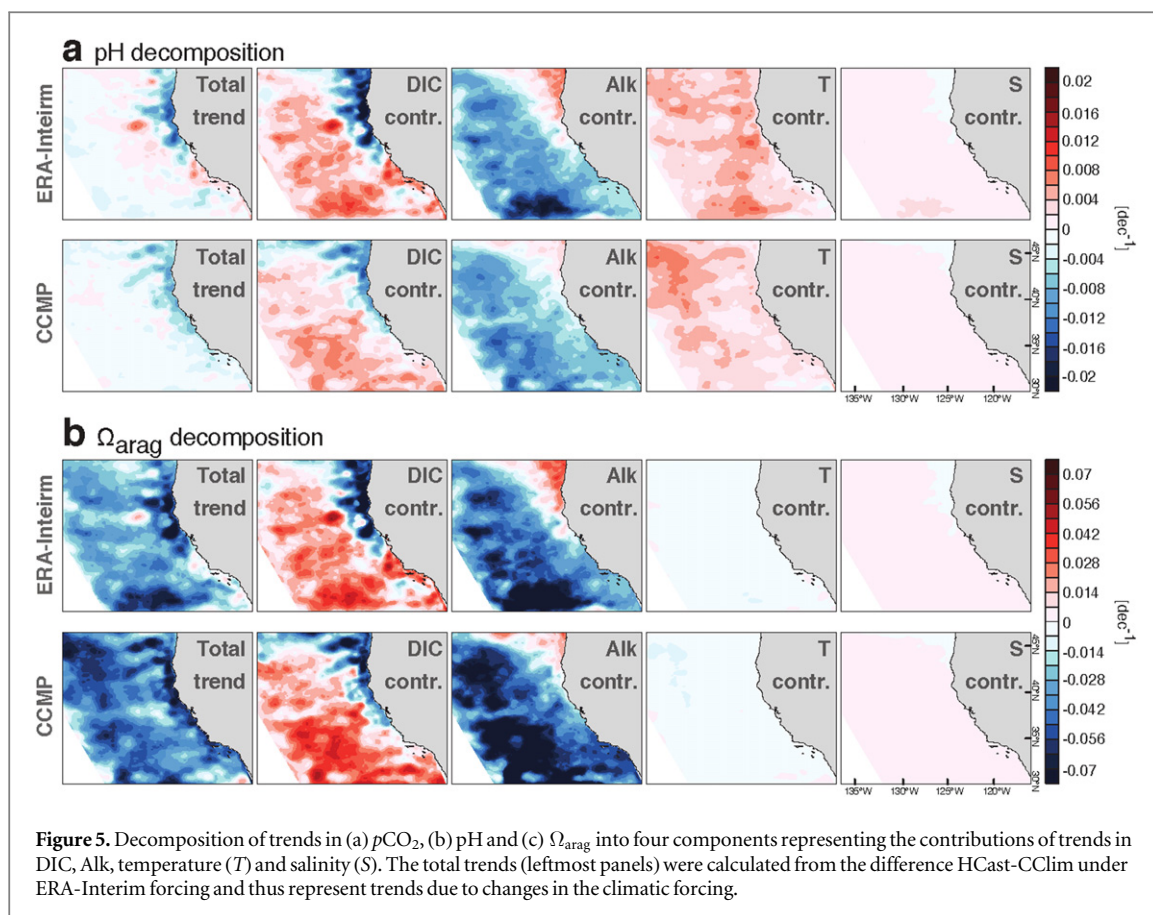


concentrations ( $[\text{CO}_3^{2-}]$ ), which could explain why the trends in  $p\text{CO}_2$ , pH,  $\Omega_{\text{arag}}$  are larger in the HCast-CCMP simulation in the offshore region as well.

A comparison of the temporal progressions of these four variables from the HCast-ERA and HCast-CCMP simulations reveals that throughout the HCast-CCMP simulation from 1988 to 2011,  $p\text{CO}_2$  is lower, pH and  $\Omega_{\text{arag}}$  are higher and  $d_{\text{as}}$  is deeper compared to the HCast-ERA simulation (figures 2(b)–(e)). Although both simulations were spun up analogously, the initial conditions for the HCast-CCMP simulations in 1988 differ from the conditions for the same year during the

HCast-ERA simulation. This discrepancy could partly explain the difference in the absolute values and trends (see methods and appendix for a more detailed description of the spinup processes).

As a result of the more rapid evolution of ocean acidification in the nearshore 100 km, the compression of habitat suitability is even more acute there in comparison to the trends across the whole domain. A more detailed quantification of the distribution of the volumes of water within a particular  $\Omega_{\text{arag}}$  range in the nearshore 100 km and within the euphotic zone (0–60 m; averaged over R1 and R2) reveals that the



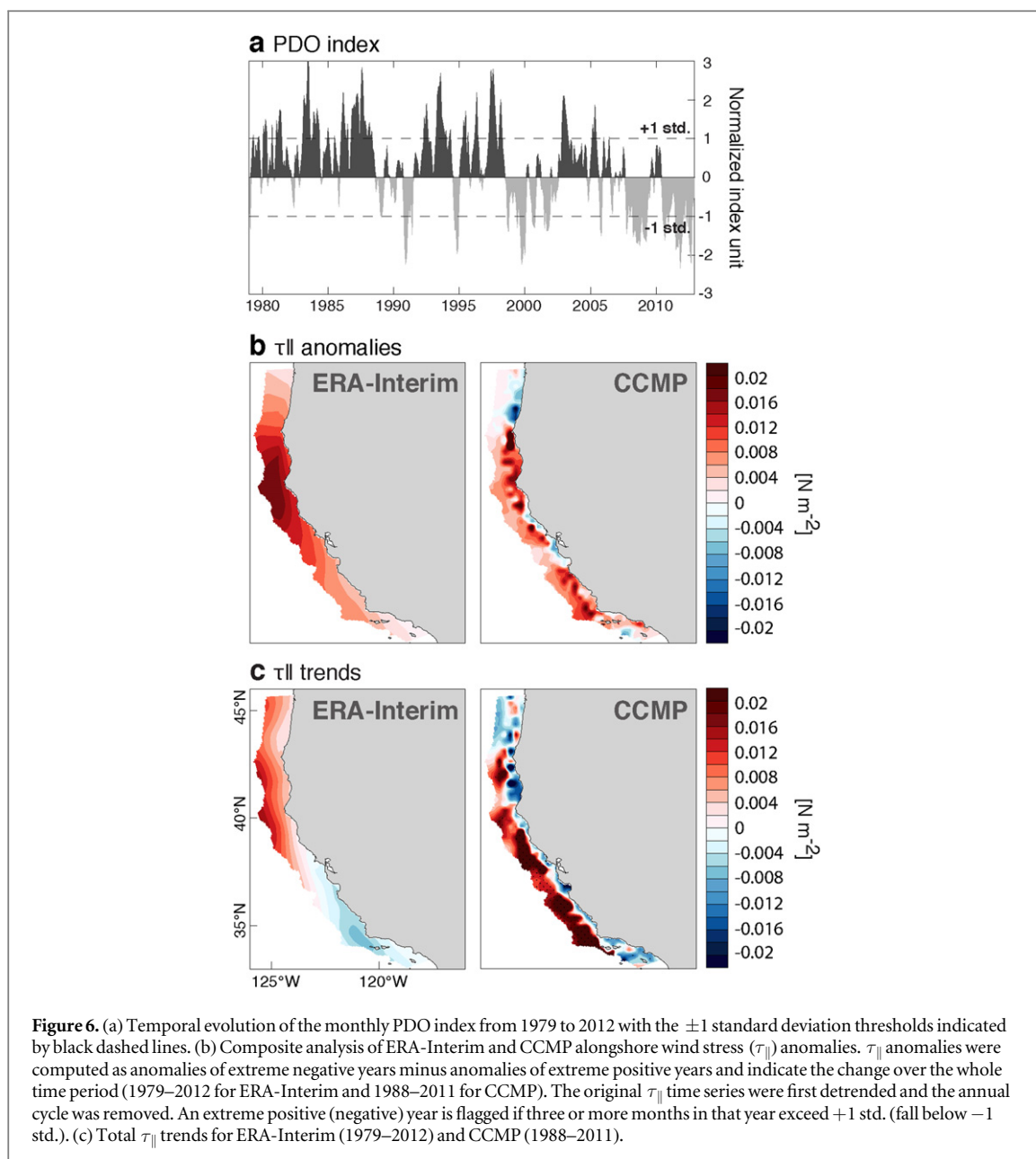
volume of water with  $\Omega_{\text{arag}} > 2$  decreased by a factor of more than two under both forcings, becoming progressively rarer (figures 3(a) and (b)). While the volume of water with  $\Omega_{\text{arag}}$  between 1.5 and 2.0 changed little, waters on the verge of undersaturation, i.e., waters with  $1 < \Omega_{\text{arag}} < 1.5$ , became much more abundant, increasing in their volume from around 10% to over 30% of the total water mass.

In the upper aphotic zone, i.e., in the layer between 60–120 m, we model in both HCast simulations a decrease of waters with  $\Omega_{\text{arag}} > 2$  to the point of disappearance by 2012 (figures 3(c) and (d)). The volume of nearly undersaturated water ( $1 < \Omega_{\text{arag}} < 1.5$ ) increases in both HCast simulations, to occupy on an annual mean up to roughly 90% (ERA-Interim) and 80% (CCMP) of the total water mass in this layer. Furthermore, toward the end of both simulations, undersaturated waters ( $\Omega_{\text{arag}} < 1$ ) start to occur on a monthly basis, occupying up to 10% of the water mass.

Strong variations in the volumes of saturated and undersaturated waters are visible for both layers of the water column on seasonal and interannual time scales. The magnitudes of both seasonal and interannual variability in the volume of nearly undersaturated water ( $1 < \Omega_{\text{arag}} < 1.5$ ) are roughly equal and range between  $\pm 5\%$  and  $\pm 15\%$ . The interannual fluctuations largely reflect the impact of changes in the upwelling of waters with low saturation states, mostly associated with the appearance of El Niño/La Niña

conditions (e.g., Frischknecht *et al* 2015, Jacox *et al* 2015).

Our reconstructed evolution of ocean acidification in the CalCS reveals that substantial changes have occurred in the last few decades and highlights that recent distributions of  $p\text{CO}_2$ , pH, and  $\Omega_{\text{arag}}$  are very different from those that characterized the system a few decades ago. These reconstructions will put other observations of changes in biogeochemistry and ecosystems into historical context and provide a basis against which future projected changes can be compared to. Gruber *et al* (2012) demonstrated for example that the volume of undersaturated water that began to appear in the nearshore area between 60 and 120 m will become the norm by 2030. They also projected the appearance of undersaturated conditions in the top 60 m within the next decade. Furthermore, Hauri *et al* (2013a) suggested that it takes 20–30 years for trends in ocean acidification to emerge from the background variability in the CalCS. This finding is consistent with our trends in  $p\text{CO}_2$ , pH,  $\Omega_{\text{arag}}$  and  $d_{\text{as}}$ , which are highly significant across the whole domain (table 1) and thus are clearly distinguishable from the sub-decadal variability. Therefore, the fundamental alteration of habitat suitability for organisms and ecosystems vulnerable to ocean acidification has begun several decades ago, and is bound to become more accentuated in the coming decades.



#### 4. Drivers of trends in ocean acidification

If the increase in atmospheric  $\text{CO}_2$  were the only driver for ocean acidification across the CalCS, one would expect a relatively uniform trend pattern. However, the substantial spatial variations in the ocean acidification trends seen in our reconstructed fields indicate a different picture. They suggest that local, yet climatically forced, processes must have modulated the purely atmospheric  $\text{CO}_2$ -driven trends in the last few decades. This strong nearshore ocean acidification signal is due to a change in the upwelling of waters that are high in natural  $\text{CO}_2$ , stemming from the remineralization of organic matter rather than an anthropogenic signal of the source waters from previous decades.

To quantify this climate variability-induced modulation in more detail, we compare the trends from the

HCast simulations to the results from the corresponding CCLim simulations, where we only allowed lateral DIC and atmospheric  $\text{CO}_2$  to vary. On average, the trends in pH,  $\Omega_{\text{arag}}$  and  $d_{\text{as}}$  in the CCLim simulations exhibit much more homogeneous patterns of change compared to the results from the corresponding HCast simulations (figures 4(a)–(f)). Given the climatological forcing, the relatively small variability in the trends from the CCLim simulations is a result of variations in the surface ocean buffer factor (Zeebe 2012) and also includes the effect of internally generated stochastic variability of the CalCS, reflecting its turbulent nature. The domain-wide changes in pH and  $\Omega_{\text{arag}}$  are similar to those from the HCast simulations, i.e., average decreases of  $-0.017 \pm 0.002 \text{ dec}^{-1}$  and  $-0.07 \pm 0.01 \text{ dec}^{-1}$ , respectively (averaged over CCLim-ERA1 and CCLim-CCMP). The shoaling rate of  $d_{\text{as}}$  of

$-13.5 \pm 3.7 \text{ m dec}^{-1}$ , however, is only about half of that from the HCast simulation.

The modulating impact of the variable climatic forcing is substantial under both forcings and occurs primarily in the nearshore regions of the CalCS (figures 4(g)–(l)). Under ERA-Interim forcing, there is a division around San Francisco Bay ( $\sim 38^\circ\text{N}$ ) in the sign of the pH trends. In the northern nearshore region (R1), variations in the climatic forcing cause a more rapid decline in pH than solely through the rise in atmospheric  $\text{CO}_2$  (50% stronger decline, see table 1), whereas in the southern nearshore region (R2) these variations dampen the atmospheric  $\text{CO}_2$ -driven trends, causing a slight increase in pH. This is also visible in the  $\Omega_{\text{arag}}$  and  $d_{\text{as}}$  trends, with a weaker decrease in  $\Omega_{\text{arag}}$  and less shoaling of  $d_{\text{as}}$  in R2 compared to R1. Under CCMP forcing, we model a more homogeneous climatic modulation of pH,  $\Omega_{\text{arag}}$  and  $d_{\text{as}}$  within the nearshore 100 km, with magnitudes of on average 60%, 125% and 200%, respectively (see table 1 for the climatic modulations).

Thus, while it is unambiguous that recent climatic variations have impacted the trends in ocean acidification across most of the coastal CalCS in a substantial manner, the details of this modulation depend on the particular forcing applied to the model. Furthermore, while the pH trends are modulated primarily in the coastal regions, the impact of the climatic variations is stronger for the trends in  $\Omega_{\text{arag}}$  and  $d_{\text{as}}$ , and extends much further offshore. This also explains the fact that the domain-wide changes in  $\Omega_{\text{arag}}$  and  $d_{\text{as}}$  differ substantially between the HCast and CCLim simulations, while in the case of pH the domain-wide trends are nearly equal.

## 5. Climatic modulation of ocean acidification

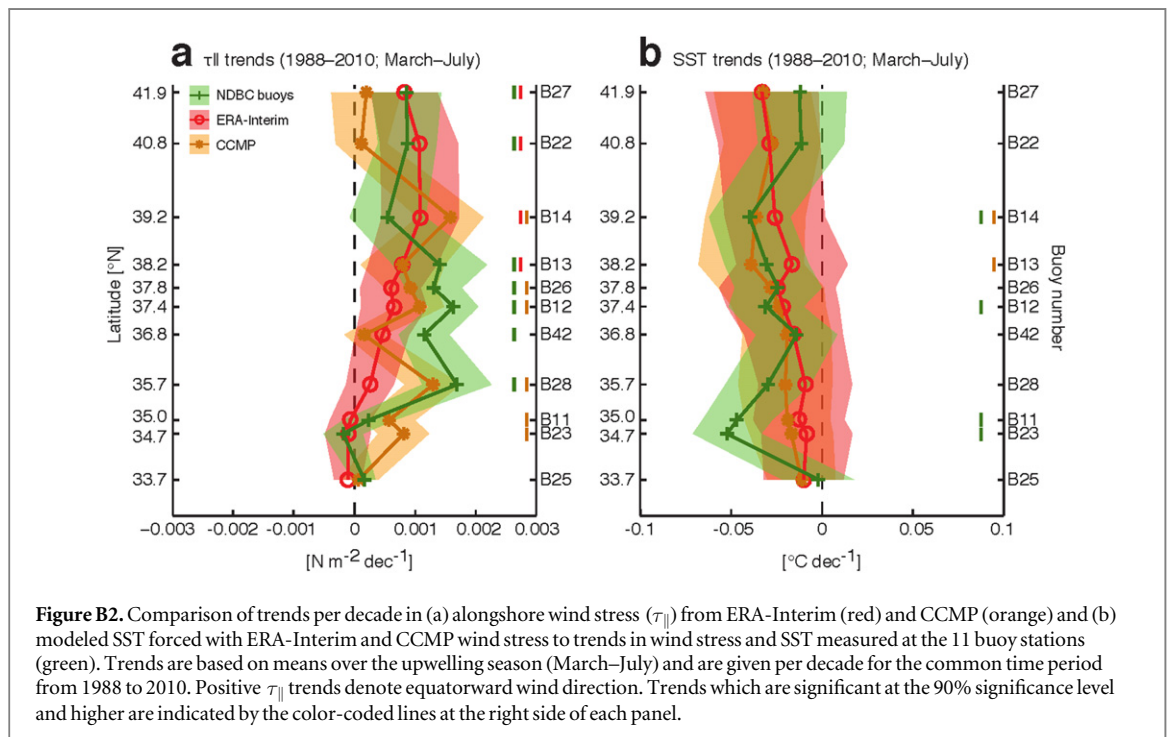
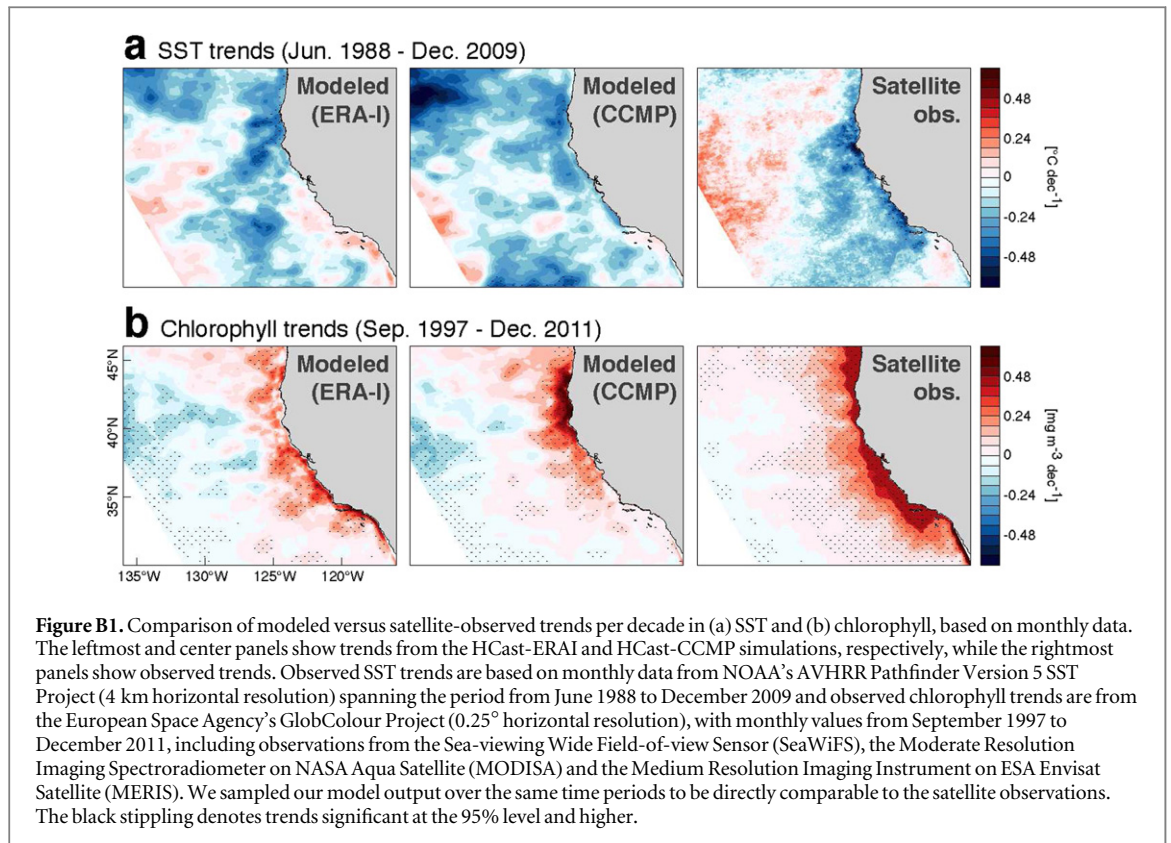
To determine the processes responsible for the climatic modulation of the trends in ocean acidification, we employ a first-order Taylor expansion of the trends in the difference HCast-CCLim averaged over the top 60 m of the water column for  $p\text{CO}_2$ , pH and  $\Omega_{\text{arag}}$ . We expand the trends into components representing trends in DIC, Alk, temperature and salinity from the difference HCast-CCLim (after Lovenduski *et al* 2007, Doney *et al* 2009, Turi *et al* 2014, see figure B3 for trends in DIC, Alk, temperature and salinity). This decomposition reveals that both under ERA-Interim and under CCMP forcing, the strong nearshore decline in pH is mainly driven by the local increase in DIC (figures 5(a) and B3(a) and (e)). The decrease in Alk and the surface cooling dampen the DIC effect to a certain extent, but are too weak to fully compensate (figures B3(b), (c), (f) and (g)). In the offshore regions, the positive effect of the decrease in Alk on pH is almost entirely balanced by the effect of the decreases in temperature and DIC. In the case of  $\Omega_{\text{arag}}$ , the

nearshore increase in DIC dominates the trends there, while the offshore decrease in Alk dominates the trends away from the coast, resulting in the almost domain-wide decrease in  $\Omega_{\text{arag}}$  (figure 5(b)). In strong contrast to the trends in pH, the effect of the domain-wide cooling is negligible for the trend in  $\Omega_{\text{arag}}$ . The contribution of trends in salinity is too small to significantly modify the trends in both pH and  $\Omega_{\text{arag}}$  (figures B3(d) and (h)). In order to assess the role of biology in driving the modeled trends in the carbonate system, we computed the changes in the sources and sinks of  $[\text{CO}_3^{2-}]$ . Our results indicated no significant trends in the biologically driven changes in  $[\text{CO}_3^{2-}]$  (not shown).

Thus, having eliminated changes in biology as an important contributor to our modeled trends, the coastal signature of the trends with nearshore high DIC and low temperatures clearly points to a change in upwelling as the dominant process underlying the climatic modulation of the ocean acidification trends. This is consistent with the alongshore wind stress trends in the forcing products (figure 6(c)). ERA-interim shows an increase in equatorward, upwelling-favorable wind stress to the north of roughly  $38^\circ\text{N}$ , whereas the trend is toward weaker equatorward wind stress to the south of this. CCMP alongshore wind stress trends are mostly positive, i.e., toward upwelling-favorable wind stress, all along the coast. This resulting pattern of increased upwelling in the northern subregion for ERA-Interim and of strong increases in upwelling along the entire coast for CCMP can explain our modeled pattern of ocean acidification due to the climatic modulation very well. This is consistent with findings from Turi *et al* (2014), who demonstrated that variations in DIC, driven by changes in circulation (i.e., upwelling), are the main driver for  $p\text{CO}_2$  variability in the nearshore 100 km of the CalCS.

The increased upwelling can also explain the much farther offshore reach of the climatic modulation for  $\Omega_{\text{arag}}$  and  $d_{\text{as}}$  relative to that of pH. This is because the stronger equatorward wind stress along the shores causes not only stronger upwelling, but also pulls the upper thermocline up, causing a shoaling of the isopycnals and the upward movement of the waters with undersaturated conditions. This thermocline shoaling extends to about 800 km offshore (not shown), explaining the wide reach of the stronger decline in  $\Omega_{\text{arag}}$  and shoaling of  $d_{\text{as}}$ .

With increased upwelling as the primary driver of the larger than expected trends, it befits us to demonstrate that these trends are reliable. A detailed comparison of the two wind products with mooring-based trend estimates (García-Reyes and Largier 2010) confirms the trends, with the CCMP wind stress data in general comparing more favorably to the *in situ* measurements (see appendix figures B1 and B2). Also the comparison of the modeled trends in SST and chlorophyll from both HCast simulations with satellite-based estimates supports our finding of substantial



trends, again with the results from the HCast-CCMP simulation obtaining better agreements. However, the simulations under CCMP forcing only cover the period from 1988 to 2011 (24 years), whereas the ERA-interim simulations extend over 34 years. Thus, the latter simulations lend themselves better to the analyzes of multi-decadal trends, i.e., are less sensitive to the choice of beginning and end years.

As pointed out previously by Chhak and Di Lorenzo (2007), the Pacific Decadal Oscillation (PDO), a leading mode of climate variability in the North Pacific region (e.g., Mantua and Hare 2002), has a significant effect on the depth of the upwelling cell in the CalCS. They found that during warm phases of the PDO, the upwelling cell is shallower, potentially limiting the supply of nutrients and DIC to the surface, whereas

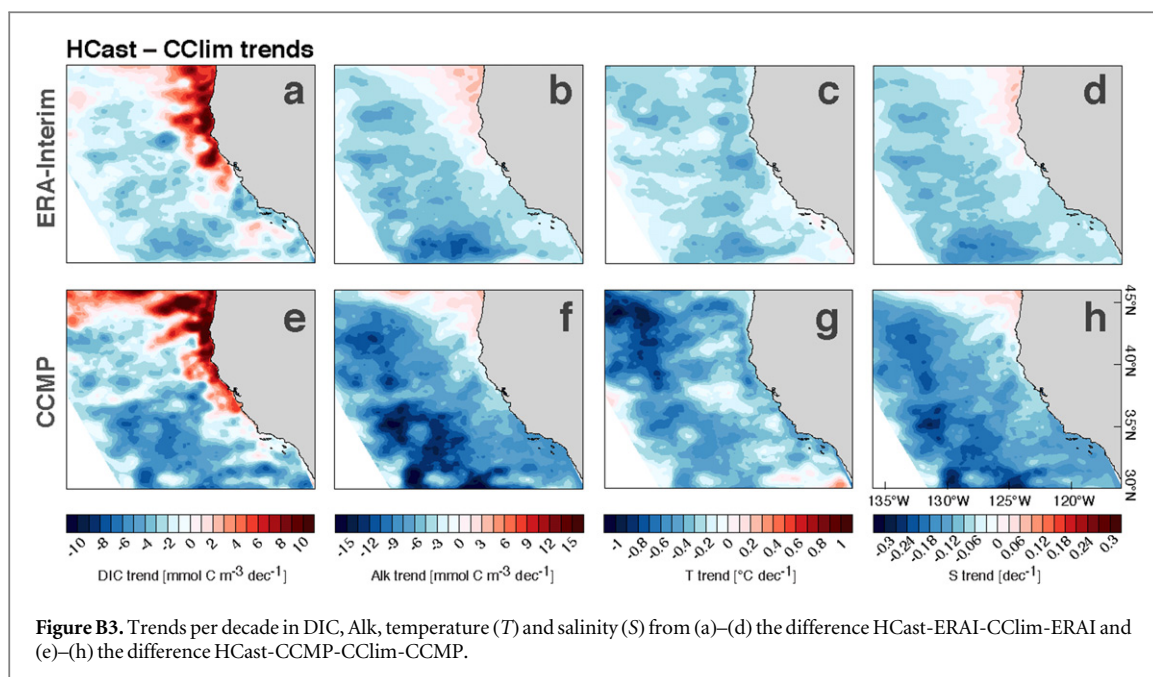


**Figure B3.** Trends per decade in DIC, Alk, temperature ( $T$ ) and salinity ( $S$ ) from (a)–(d) the difference HCast-ERA-Interim-CCLim-ERA-Interim and (e)–(h) the difference HCast-CCMP-CCLim-CCMP.

during cool phases, the opposite is the case. The PDO was predominantly in a warm phase at the beginning of our simulation (roughly 1979–1988; figure 6(a)), progressing to a cool phase toward the end of our simulation (roughly 2008–2012). A composite analysis of detrended annual mean alongshore wind stress with the PDO index highlights that during cool phases of the PDO, the nearshore 100 km of the CalCS experiences positive, equatorward wind stress anomalies of up to  $0.02 \text{ N m}^{-2}$  larger than during warm phases, both in the case of ERA-Interim and CCMP (figure 6(b)). As these anomalies are on the order of the total trends over the whole simulation (figure 6(c)), the observed transition from a warm to a cool phase of the PDO over this time period could serve as a possible explanation for the observed trend toward more upwelling-favorable alongshore wind stress. The study by Feely *et al* (2012) found a shoaling of the aragonite saturation depth in the CalCS to depths of around  $-150 \text{ m}$  over a 10 year period between 1994 and 2004. Around the same depth they also found an increase in cool,  $\text{CO}_2$ -rich waters, which was consistent with measurements by Di Lorenzo *et al* (2005), who found a cooling and freshening of waters in the southern CalCS, which they attributed to an increase in southward advection of waters with those properties. These results support our finding that a combination of physical and chemical properties affect the carbonate system of the CalCS and that local changes in circulation can contribute significantly to ocean acidification, in addition to the direct effect of rising atmospheric  $\text{CO}_2$ .

Without a proper attribution, however, it is not possible to determine whether these trends in the alongshore wind stress are primarily the result of unforced variations of the climate system related to the PDO and to other modes of climate variability, or

whether they are indeed fingerprints of ongoing anthropogenic climate change, as has been alluded to by a number of studies in recent decades (e.g., Bakun 1990, Diffenbaugh *et al* 2004, Narayan *et al* 2010, Sydeman *et al* 2014, Wang *et al* 2015).

## 6. Summary and conclusions

We used two sets of simulations from an eddy-resolving ocean biogeochemical model of the CalCS forced with two different wind products to (i) reconstruct trends in ocean acidification from 1979 to 2012 and (ii) separate the effects of the recent increase in atmospheric  $\text{CO}_2$  and of changes in the climatic forcing on these trends. To this end, we compared a simulation with fully transient atmospheric forcing and lateral boundary conditions (‘HCast’) to a simulation where only atmospheric  $\text{CO}_2$  and lateral DIC were allowed to vary (‘CCLim’).

Irrespective of the forcing product, our model reconstructs domain-wide decreases in surface ocean pH and  $\Omega_{\text{arag}}$  that correspond roughly to those seen in the global ocean. In addition, we model a rapid shoaling of the depth of the saturation horizon. Across the entire domain it is found to have moved upward at a rate of  $-28$  to  $-38 \text{ m dec}^{-1}$ , leading to a rapid compression of the volume of waters that are supersaturated with regard to aragonite.

The most severe changes in ocean acidification occur in an area limited to the first 100 km along the coast. In the case of the HCast-ERA-Interim simulation, this area is located roughly between San Francisco Bay and Cape Blanco, Oregon ( $\sim 38$ – $43^\circ\text{N}$ ), whereas in the HCast-CCMP simulation the area of maximum trends is more widespread ( $\sim 35$ – $45^\circ\text{N}$ ). In these areas, ocean acidification has been progressing at rates up to 30%

faster than what is found for the whole domain. This caused a more rapid emergence of undersaturated waters with respect to aragonite than would have been expected on the basis of the trends in atmospheric  $\text{CO}_2$  alone. Furthermore, the upwelling of waters high in natural  $\text{CO}_2$  that has accumulated at depth over time, masks any anthropogenic signal of the source waters of the CalCS, which would carry a lower  $\text{CO}_2$  signal from decades prior to upwelling.

While there existed essentially no undersaturated waters with respect to aragonite ( $\Omega_{\text{arag}} < 1$ ) in the upper aphotic zone (60–120 m) of the nearshore 100 km in the late 1970s, such water masses can now occupy up to 10% of the total water mass of this layer. These strong historical changes in the biogeochemical habitat are bound to have had an effect on organisms and ecosystems that are potentially vulnerable to ocean acidification. There exist only a handful of studies that have looked at longer-term changes in organisms and ecosystems and related them to ocean acidification (e.g., Ohman *et al* 2009, Mackas and Galbraith 2012, Bednaršek *et al* 2014, Bednaršek and Ohman 2015) and the records are generally sparse in space and time and are often confounded by additional impacts such as warming and changes in oceanic productivity (e.g., Breitburg *et al* 2015). However, our results suggest that the observation by Bednaršek *et al* (2014) of pteropods with significant signs of dissolution in the upper ocean of the northern coastal region is a recent phenomenon. Our reconstructed history of ocean acidification in the CalCS will hopefully help undertake more historical impact assessments.

While averaged over the entire domain, the main driver of the trends in ocean acidification is the invasion of anthropogenic  $\text{CO}_2$  from the atmosphere into the ocean, climatic fluctuations substantially modulated these trends regionally, particularly in the nearshore 100 km. Specifically, in the northern coastal subregion, the climatic modulation caused a 50% stronger increase in  $p\text{CO}_2$  and decrease in pH than expected only from the increase in atmospheric  $\text{CO}_2$ . In the same region, the decrease in  $\Omega_{\text{arag}}$  and shoaling of the aragonite saturation depth due to changes in the climatic forcing were two to three times above the purely atmospheric  $\text{CO}_2$ -driven trends. These modulations are largely driven by a strong nearshore DIC increase caused by a trend toward increased upwelling, which itself is possibly linked to a negative trend of the PDO. It remains to be determined whether these changes simply reflect ‘natural’, i.e., unforced fluctuations of the climate system or whether they are the first signs of anthropogenic climate change. If it is the latter, then one can expect ocean acidification to continue advancing more rapidly than expected in the nearshore areas of the CalCS. If the former is the case, such past periods of rapid acidification will be followed by periods of moderate increase.

This modeling study is the first to investigate separately the effects of increasing atmospheric  $\text{CO}_2$  and of changes in the climatic forcing on ocean acidification in the CalCS. Our model results show a clear connection between a local increase in upwelling-favorable wind stress and a significant modulation of purely atmospheric  $\text{CO}_2$ -driven ocean acidification in the nearshore 100 km. It is undeniable that amplified local ocean acidification in the CalCS, as simulated in this study, has a deleterious impact on calcifying organisms by reducing the saturation state of  $\Omega_{\text{arag}}$  to a point of waters being corrosive to the organisms’ shells and skeletons (e.g., Feely *et al* 2008, Bednaršek *et al* 2014). Thus, our study demonstrates the importance of considering changes in the climatic forcing, particularly changes in upwelling-favorable wind stress, in addition to the influence of rising atmospheric  $\text{CO}_2$  on ocean acidification in coastal upwelling regions.

## Acknowledgments

This research was funded by ETH Zürich and through the EU FP7 projects CARBOCHANGE and GEOCARBON, which received financial support from the European Commission’s Seventh Framework Programme (FP7/2007–2013) under grant agreements n° 264879 and 283080, respectively. The simulations in this study were performed largely by Damian Loher, whose assistance and support we are very thankful for, at the central computing clusters Brutus and Euler of ETH Zürich. The ERA-Interim reanalysis data used in this study were downloaded from the ECMWF Data Server (<http://ecmwf.int/en/research/climate-reanalysis/ERA-interim>) and the CCMP wind speed data were obtained from NASA’s Physical Oceanography Distributed Active Archive Center ([http://podaac.jpl.nasa.gov/Cross-Calibrated\\_Multi-Platform\\_OceanSurfaceWindVectorAnalyses](http://podaac.jpl.nasa.gov/Cross-Calibrated_Multi-Platform_OceanSurfaceWindVectorAnalyses)). We are grateful to M García-Reyes for sharing the buoy measurements that we used for our model evaluation and which were obtained from NOAA’s National Data Buoy Center (<http://ndbc.noaa.gov/>). The PDO index monthly time series was downloaded from the Joint Institute for the Study of the Atmosphere and the Ocean (<http://jisao.washington.edu/pdo/>).

## Appendix A. Model details

For both HCast and CCLim simulations, we used monthly atmospheric  $\text{CO}_2$  concentrations from the Earth System Research Laboratory’s GLOBALVIEW- $\text{CO}_2$  data set (Cooperative Global Atmospheric Data Integration Project 2013) from 1979 to 2012 and averaged latitudinally from 24°N to 48°N to obtain domain-mean values. To convert GLOBALVIEW’s mole fraction of  $\text{CO}_2$  to  $p\text{CO}_2$ , we used monthly atmospheric surface pressure, temperature and relative humidity from ERA-Interim. To cover the spinup

period from 1969 to 1978, we linearly extended the GLOBALVIEW-CO<sub>2</sub> time series to the ten years prior to its starting date based on monthly data over the period 1979–2012. This reconstructed marine boundary layer value for our mean latitude differs relatively little from the direct observations of the atmospheric CO<sub>2</sub> mixing ratio from Cape Kumakahi, Hawaii (Keeling *et al* 2009).

For the CCLim simulations, the lateral temperature and salinity boundary conditions are climatologies derived from the Simple Ocean Data Assimilation (SODA) database (Chepurin *et al* 2005), whereas nutrients and oxygen are taken from the World Ocean Atlas 2005 (Antonov *et al* 2006, Garcia *et al* 2006a, 2006b, Locarnini *et al* 2006). Chlorophyll, phytoplankton and zooplankton lateral boundary conditions are monthly climatologies derived from SeaWiFS, using the algorithms of Gruber *et al* (2006) to estimate phytoplankton and zooplankton biomass throughout the upper ocean from the remotely sensed surface chlorophyll. The DIC and Alk boundary conditions are monthly climatologies derived from the Global Ocean Data Analysis Project (Key *et al* 2004), using a seasonal regression for Alk and the seasonal cycle of *p*CO<sub>2</sub> from Takahashi *et al* (2009) to reconstruct monthly variations in DIC and Alk. We applied the same bias correction to the climatological DIC boundary conditions as described in Turi *et al* (2014).

To obtain transient conditions at the lateral boundaries for the HCast simulations, we added monthly anomalies from a hindcast simulation performed by Graven *et al* (2012) to our monthly climatological boundary conditions. These simulations were performed using the National Center for Atmospheric Research Community Climate System Model version 3.0 (CCSM3; Collins *et al* 2006, Gent *et al* 2006, Smith *et al* 2010) and were forced with the Common Ocean–ice Reference Experiments–Corrected Inter–Annual Forcing (CORE-CIAF; Large and Yeager 2004). In the case of the CCLim simulations, the climatological DIC boundary conditions were superimposed with anomalies based on a CCSM3 simulation forced with the Common Ocean–ice Reference Experiments–Corrected Normal Year Forcing (CORE-CNYF; Gent *et al* 2006). As the CCSM3 simulations by Graven *et al* (2012) only span the period from 1760 to 2007, we extended them to the end of 2009 (i.e., to the end of the CORE-CIAF data period), and repeated the forcing of the year 2009 to match the ERA-Interim period, which ends in 2012.

## Appendix B. Model evaluation with satellite and *in situ* observations

To test the model's performance under two different wind products, we compare modeled SST and chlorophyll from our HCast simulations to satellite observations from NOAA's AVHRR Pathfinder Version 5

SST Project and ESA's GlobColour Project, respectively (figure B1). Both under ERA-Interim and under CCMP forcing, our model simulates a stronger cooling throughout the north of the model domain compared to satellite-observed SST (figure B1(a)). In the areas offshore of roughly 500 km, the HCast-ERA simulation compares more favorably to the observations and manages to capture the nearshore decrease and offshore increase in SST fairly well. On the other hand, the HCast-CCMP simulation does a better job of modeling the decrease in SST throughout the nearshore 100 km, which is our primary region of interest. The overestimation of SST in the nearshore areas south of roughly 40°N by the HCast-ERA simulation could lead to a slight modification of our results presented in figure 5. Too high SST values could lead to too high (too low) *p*CO<sub>2</sub> (pH), and thus increase the north–south gradient in both *p*CO<sub>2</sub> and pH trends. The comparison of the trends in the modeled and satellite-observed chlorophyll shows that under ERA-interim forcing, the modeled trends throughout the nearshore 100 km are only roughly half as large as the observed trends (figure B1(b)). The HCast-CCMP simulation on the other hand fails to capture the strong positive chlorophyll trend south of roughly 40° N, but simulates well the strong cross-shore gradients in chlorophyll trends to the north of this. An underestimation of chlorophyll in the nearshore area by the model could indicate an underrepresentation of upwelling due to too weak alongshore winds, which would imply that the local, nearshore amplification of ocean acidification might be even larger than our results in figures 1 and 4 suggest. In conclusion, although the HCast-ERA simulation captures well the latitudinal extent of the strong increase in chlorophyll all along the coast, on average, for both SST and chlorophyll, the HCast-CCMP simulation compares more favorably to the satellite measurements in the nearshore 100 km in terms of absolute magnitude.

To further evaluate ERA-Interim and CCMP wind stress data and the model's behavior under different forcings, we compare trends in alongshore wind stress ( $\tau_{\parallel}$ ) from these two products and modeled SST trends to measured  $\tau_{\parallel}$  and SST trends from a set of eleven buoys along the US west coast (figure B2). The buoy data were provided to us directly by García-Reyes who obtained them from NOAA's National Data Buoy Center. We focus on the modeled and observed data's common time period from 1988 to 2010 and calculate trends based on the upwelling season from March to July (as in García-Reyes and Largier 2010). To compute the  $\tau_{\parallel}$  component, we use monthly mean *u*- and *v*-momentum wind stress and our model's coastal angle due north, which we smoothed using the 'LOESS' method based on a weighted quadratic least squares regression to account for the coarser resolution of our wind forcing products as compared to the topography.

In the case of ERA-Interim, the strongest  $\tau_{||}$  trends occur locally around Cape Mendocino ( $\sim 40^{\circ}\text{N}$ ), whereas trends in CCMP  $\tau_{||}$  show a much more variable pattern along the coast, with very local increases and decreases of up to an order of magnitude larger than ERA-Interim  $\tau_{||}$  trends (figure 6(c)). Seven of the eleven buoys show a significant ( $> 90\%$  significance level) increase in  $\tau_{||}$  in the area from roughly  $35^{\circ}\text{N}$  to  $38^{\circ}\text{N}$  and north of  $40^{\circ}\text{N}$  (figure B2(a)). ERA-Interim  $\tau_{||}$  trends compare favorably to the buoy data north of  $38^{\circ}\text{N}$ , with significant trends in the four northernmost buoys. Between  $35^{\circ}\text{N}$  to  $38^{\circ}\text{N}$  however, ERA-Interim  $\tau_{||}$  trends are considerably smaller than the observed trends, leading us again to the conclusion that upwelling might be underestimated in this particular region in the HCast-ERAI simulation. In contrast, trends in CCMP  $\tau_{||}$  better capture the latitudinal variability, which is also visible in the buoy  $\tau_{||}$  trends. However, CCMP  $\tau_{||}$  trends compare less favorably to the buoy data at the two northernmost buoy locations (B22 and B27) and further south at locations B11 and B23. In conclusion, ERA-Interim  $\tau_{||}$  trends appear to be more consistent with *in situ* observations North of  $38^{\circ}\text{N}$  and south of roughly  $35^{\circ}\text{N}$ , whereas CCMP  $\tau_{||}$  trends compare more favorably to the buoy data in between. Trends in modeled SST, both under ERA-Interim and under CCMP forcing, agree on average well with the buoy trends (figure B2(b)): the signs of the modeled trends are in agreement with the observed trends for all buoys and—with the exception of buoys B11 and B23—the magnitude of the negative trends are within the error margins.

## References

- Alin S R, Feely R A, Dickson A G, Martín Hernández-Ayón J, Juranek L W, Ohman M D and Goericke R 2012 Robust empirical relationships for estimating the carbonate system in the Southern California Current System and application to CalCOFI hydrographic cruise data (2005–2011) *J. Geophys. Res.* **117** C05033
- Antonov J I, Locarnini R A, Boyer T P, Mishonov A V and Garcia H E 2006 *World Ocean Atlas 2005, Volume 2: Salinity* ed S Levitus, NOAA Atlas NESDIS 62 (Washington, DC: U.S. Government Printing Office) ([ftp://ftp.nodc.noaa.gov/pub/WOA05/DOC/woa05\\_salinity\\_final.pdf](ftp://ftp.nodc.noaa.gov/pub/WOA05/DOC/woa05_salinity_final.pdf)) p 182
- Atlas R, Hoffman R N, Ardizzone J, Leidner S M, Jusem J C, Smith D K and Gombos D 2011 A cross-calibrated, multiplatform ocean surface wind velocity product for meteorological and oceanographic applications *Bull. Am. Meteorol. Soc.* **92** 157–74
- Bakun A 1990 Global climate change and intensification of coastal ocean upwelling *Science* **247** 198–201
- Barton A, Hales B, Waldbusser G G, Langdon C and Feely R A 2012 The Pacific oyster, *Crassostrea gigas*, shows negative correlation to naturally elevated carbon dioxide levels: implications for near-term ocean acidification effects *Limnology Oceanogr.* **57** 698–710
- Barton A *et al* 2015 Impacts of coastal acidification on the Pacific Northwest shellfish industry and adaptation strategies implemented in response *Oceanography* **28** 146–59
- Bates R N, Astor Y M, Church M J, Currie K, Dore J E, González-Dávila M, Lorenzoni L, Muller-Karger F, Olafsson J and Santana-Casiano J M 2014 A time-series view of changing surface ocean chemistry due to ocean uptake of anthropogenic  $\text{CO}_2$  and ocean acidification *Oceanography* **27** 126–41
- Bednaršek N, Feely R A, Reum J C P, Peterson B, Menkel J, Alin S R and Hales B 2014 *Limacina helicina* shell dissolution as an indicator of declining habitat suitability owing to ocean acidification in the California current ecosystem *Proc. R. Soc. B* **281** 20140123
- Bednaršek N and Ohman M D 2015 Changes in pteropod distributions and shell dissolution across a frontal system in the California current system *Mar. Ecology Prog. Ser.* **523** 93–103
- Borges A V *et al* 2009 A global sea surface carbon observing system: inorganic and organic carbon dynamics in coastal oceans *Proc. 'OceanObs'09: Sustained Ocean Observations and Information for Society' Conf. vol 2* ([www.oceanobs09.net/proceedings/cwp/Borges-OceanObs09.cwp.07.pdf](http://www.oceanobs09.net/proceedings/cwp/Borges-OceanObs09.cwp.07.pdf))
- Breitbart D L *et al* 2015 And on top of all that... coping with ocean acidification in the midst of many stressors *Oceanography* **28** 48–61
- Byrne R H, Mecking S, Feely R A and Liu X 2010 Direct observations of basin-wide acidification of the North Pacific Ocean *Geophys. Res. Lett.* **37** 1–5
- Cai W-J *et al* 2011 Acidification of subsurface coastal waters enhanced by eutrophication *Nat. Geosci.* **4** 766–70
- Chepurin G A, Carton J A and Dee D 2005 Forecast model bias correction in ocean data assimilation *Mon. Weather Rev.* **133** 1328–42
- Chhak K and Di Lorenzo E 2007 Decadal variations in the California current upwelling cells *Geophys. Res. Lett.* **34** L14604
- Collins W D *et al* 2006 The community climate system model version 3 (CCSM3) *J. Clim.* **19** 2122–43
- Cooperative Global Atmospheric Data Integration Project 2013 Multi-laboratory compilation of synchronized and gap-filled atmospheric carbon dioxide records for the period 1979–2012 (obspack\_co2\_1\_GLOBALVIEW-CO2\_2013\_v1.0.4\_2013-12-23) (Boulder, CO: NOAA Global Monitoring Division) (doi:10.334/OBSPACK/1002)
- Dee D P *et al* 2011 The ERA-Interim reanalysis: configuration and performance of the data assimilation system *Q. J. R. Meteorol. Soc.* **137** 553–97
- Demarcq H 2009 Trends in primary production, sea surface temperature and wind in upwelling systems (1998–2007) *Prog. Oceanogr.* **83** 376–85
- Diffenbaugh N S, Snyder M A and Sloan L C 2004 Could  $\text{CO}_2$ -induced land-cover feedbacks alter near-shore upwelling regimes? *Proc. Natl Acad. Sci. USA* **101** 27–32
- Di Lorenzo E, Miller A J, Schneider N and McWilliams J C 2005 The warming of the California current system: dynamics and ecosystem implications *J. Phys. Oceanogr.* **35** 336–62
- Doney S C, Lima I, Feely R A, Glover D M, Lindsay K, Mahowald N, Moore J K and Wanninkhof R 2009 Mechanisms governing interannual variability in upper-ocean inorganic carbon system and air–sea  $\text{CO}_2$  fluxes: physical climate and atmospheric dust *Deep-Sea Res. II* **56** 640–55
- Doney S C, Mahowald N, Lima I, Feely R A, Mackenzie F T, Lamarque J-F and Rasch P J 2007 Impact of anthropogenic atmospheric nitrogen and sulfur deposition on ocean acidification and the inorganic carbon system *PNAS* **104** 14580–5
- Duarte C M, Hendriks I E, Moore T S, Olsen Y S, Steckbauer A, Ramajo L, Carstensen J, Trotter J A and McCulloch M 2013 Is ocean acidification an open-ocean syndrome? Understanding anthropogenic impacts on seawater pH *Estuaries Coasts* **36** 221–36
- Fay A R and McKinley G A 2013 Global trends in surface ocean p  $\text{CO}_2$  from *in situ* data *Global Biogeochemical Cycles* **27** 541–57
- Feely R A, Doney S C and Cooley S R 2009 Ocean acidification: present conditions and future changes in a high- $\text{CO}_2$  world *Oceanography* **22** 36–47
- Feely R A, Sabine C L, Byrne R H, Millero F J, Dickson A G, Wanninkhof R, Murata A, Miller L A and Greeley D 2012 Decadal changes in the aragonite and calcite saturation state of the Pacific ocean *Global Biogeochemical Cycles* **26** 1–5

- Feely RA, Sabine CL, Hernandez-Ayon JM, Janson D and Hales B 2008 Evidence for upwelling of corrosive acidified water onto the continental shelf *Science* **320** 1490–2
- Feely RA, Sabine CL, Lee K, Berelson W, Kleypas J, Fabry V J and Millero F J 2004 Impact of anthropogenic CO<sub>2</sub> on the CaCO<sub>3</sub> system in the oceans *Science* **305** 362–6
- Frieder CA, Nam SH, Martz TR and Levin LA 2012 High temporal and spatial variability of dissolved oxygen and pH in a nearshore California kelp forest *Biogeosciences* **9** 3917–30
- Frischknecht M, Münnich M and Gruber N 2015 Remote versus local influence of ENSO on the California current system *J. Geophys. Res.* **120** 1353–74
- Garcia HE, Locarnini RA, Boyer TP and Antonov JI 2006a *World Ocean Atlas 2005, Volume 3: Dissolved Oxygen, Apparent Oxygen Utilization and Oxygen Saturation* ed S Levitus NOAA Atlas NESDIS 63 (Washington, DC: U.S. Government Printing Office) p 342 ([ftp://ftp.nodc.noaa.gov/pub/WOA05/DOC/woa05\\_oxygen\\_final.pdf](ftp://ftp.nodc.noaa.gov/pub/WOA05/DOC/woa05_oxygen_final.pdf))
- Garcia HE, Locarnini RA, Boyer TP and Antonov JI 2006b *World Ocean Atlas 2005, Volume 4: Nutrients (Phosphate, Nitrate, Silicate)* ed S Levitus NOAA Atlas NESDIS 64 (Washington, DC: U.S. Government Printing Office) p 396 ([ftp://ftp.nodc.noaa.gov/pub/WOA05/DOC/woa05\\_nutrients\\_final.pdf](ftp://ftp.nodc.noaa.gov/pub/WOA05/DOC/woa05_nutrients_final.pdf))
- García-Reyes M and Largier J 2010 Observations of increased wind-driven coastal upwelling off central California *J. Geophys. Res.* **115** C04011
- Gent PR, Bryan FO, Danabasoglu G, Lindsay K, Tsumumne D, Hecht MW and Doney SC 2006 Ocean chlorofluorocarbon and heat uptake during the twentieth century in the CCSM3 *J. Clim.* **19** 2366–81
- Graven HD, Gruber N, Key R, Khatiwala S and Giraud X 2012 Changing controls on oceanic radiocarbon: new insights on shallow-to-deep ocean exchange and anthropogenic CO<sub>2</sub> uptake *J. Geophys. Res.* **117** C10005
- Gruber N 2011 Warming up, turning sour, losing breath: ocean biogeochemistry under global change *Phil. Trans. R. Soc. A* **369** 1980–96
- Gruber N, Frenzel H, Doney SC, Marchesiello P, McWilliams JC, Moisan JR, Oram JJ, Plattner G-K and Stolzenbach KD 2006 Eddy-resolving simulation of plankton ecosystem dynamics in the California current system *Deep-Sea Res. I* **53** 1483–516
- Gruber N, Hauri C, Lachkar Z, Loher D, Frölicher TL and Plattner G-K 2012 Rapid progression of ocean acidification in the California current system *Science* **337** 220–3
- Harris KE, DeGrandpre MD and Hales B 2013 Aragonite saturation state dynamics in a coastal upwelling zone *Geophys. Res. Lett.* **40** 2720–5
- Hauri C, Gruber N, McDonnell AMP and Vogt M 2013a The intensity, duration, and severity of low aragonite saturation state events on the California continental shelf *Geophys. Res. Lett.* **40** 3424–8
- Hauri C, Gruber N, Plattner G-K, Alin S, Feely RA, Hales B and Wheeler P A 2009 Ocean acidification in the California current system *Oceanography* **22** 60–71
- Hauri C, Gruber N, Vogt M, Doney SC, Feely RA, Lachkar Z, Leinweber A, McDonnell A, Münnich M and Plattner G-K 2013b Spatiotemporal variability and long-term trends of ocean acidification in the California Current System *Biogeosciences* **10** 193–216
- Hersbach H 2011 Sea surface roughness and drag coefficient as functions of neutral wind speed *J. Phys. Oceanogr.* **41** 247–51
- Hofmann EE *et al* 2011 Modeling the dynamics of continental shelf carbon *Annu. Rev. Mar. Sci.* **3** 93–122
- Jacox M G, Fiechter J, Moore AM and Edwards CA 2015 ENSO and the California Current coastal upwelling response *J. Geophys. Res.* **120** 1691–702
- Jacox M G, Moore AM, Edwards CA and Fiechter J 2014 Spatially resolved upwelling in the California Current System *Geophys. Res. Lett.* **41** 3189–96
- Juranek LW, Feely RA, Peterson WT, Alin SR, Hales B, Lee K, Sabine CL and Peterson J 2009 A novel method for determination of aragonite saturation state on the continental shelf of central Oregon using multi-parameter relationships with hydrographic data *Geophys. Res. Lett.* **36** L24601
- Kahru M, Kudela R, Manzano-Sarabia M and Mitchell BG 2009 Trends in primary production in the California current detected with satellite data *J. Geophys. Res.* **114** C02004
- Kahru M, Kudela RM, Manzano-Sarabia M and Mitchell BG 2012 Trends in the surface chlorophyll of the California Current: Merging data from multiple ocean color satellites *Deep-Sea Res. II* **77–80** 89–98
- Keeling R, Piper S, Bollenbacher A and Walker J 2009 Atmospheric CO<sub>2</sub> records from sites in the SIO air sampling network *Trends: A Compendium of Data on Global Change* (Oak Ridge, TN: Carbon Dioxide Information Analysis Center, Oak Ridge National Laboratory, US Department of Energy) (doi:10.3334/CDIAC/atg.035)
- Key RM, Kozyr A, Sabine CL, Lee K, Wanninkhof R, Bullister JL, Feely RA, Millero FJ, Mordy C and Peng T-H 2004 A global ocean carbon climatology: results from global data analysis project (GLODAP) *Global Biogeochemical Cycles* **18** GB4031
- Lachkar Z 2014 Effects of upwelling increase on ocean acidification in the California and Canary current systems *Geophys. Res. Lett.* **41** 90–5
- Large WG and Yeager SG 2004 Diurnal to decadal global forcing for ocean and sea-ice models: the data sets and flux climatologies *Technical Report* NCAR/TN-460+STR, National Center for Atmospheric Research, Boulder, Colorado ([www.clivar.org/sites/default/files/documents/wgomd/Large%202526Yeager2004.pdf](http://www.clivar.org/sites/default/files/documents/wgomd/Large%202526Yeager2004.pdf))
- Lauvset SK, Gruber N, Landschützer P, Olsen A and Tjiputra J 2015 Trends and drivers in global surface ocean pH over the past 3 decades *Biogeosciences* **12** 1285–98
- Leinweber A and Gruber N 2013 Variability and trends of ocean acidification in the Southern California current system: a timeseries from Santa Monica Bay *J. Geophys. Res.* **118** 3622–33
- Lenton A, Tilbrook B, Matear RJ, Sasse T and Nojiri Y 2015 Historical reconstruction of ocean acidification in the Australian region *Biogeosciences Discuss.* **12** 8265–97
- Locarnini RA, Mishonov AV, Antonov JI, Boyer TP and Garcia HE 2006 *World Ocean Atlas 2005, Volume 1 Temperature* ed S Levitus NOAA Atlas NESDIS 61 (Washington, DC: U.S. Government Printing Office) p 182 ([ftp://ftp.nodc.noaa.gov/pub/WOA05/DOC/woa05\\_temperature\\_final.pdf](ftp://ftp.nodc.noaa.gov/pub/WOA05/DOC/woa05_temperature_final.pdf))
- Lovenduski NS, Gruber N, Doney SC and Lima ID 2007 Enhanced CO<sub>2</sub> outgassing in the Southern Ocean from a positive phase of the Southern Annular Mode *Global Biogeochemical Cycles* **21** GB2026
- Mackas DL and Galbraith MD 2012 Pteropod time-series from the NE Pacific *ICES J. Mar. Sci.* **69** 448–59
- Mantua NJ and Hare SR 2002 The Pacific decadal oscillation *J. Oceanogr.* **58** 35–44
- Marchesiello P, McWilliams JC and Shchepetkin A 2003 Equilibrium structure and dynamics of the California current system *J. Phys. Oceanogr.* **33** 753–83
- Mendelssohn R and Schwing FB 2002 Common and uncommon trends in SST and wind stress in the California and Peru–Chile current systems *Prog. Oceanogr.* **53** 141–62
- Narayan N, Paul a, Mulitza S and Schulz M 2010 Trends in coastal upwelling intensity during the late 20th century *Ocean Sci.* **6** 815–23
- Ohman MD, Lavaniegos BE and Townsend AW 2009 Multi-decadal variations in calcareous holozooplankton in the California Current System: thecosome pteropods, heteropods, and foraminifera *Geophys. Res. Lett.* **36** 2–6
- Orr JC, Najjar R, Sabine CL and Joos F 2000 Abiotic-HOWTO. Internal OCMIP report *Technical Report* LSCE/CEA Saclay, Gif-sur-Yvette, France ([www.cgd.ucar.edu/ocmip/HOWTO-Abiotic.ps](http://www.cgd.ucar.edu/ocmip/HOWTO-Abiotic.ps))
- Orr JC *et al* 2005 Anthropogenic ocean acidification over the twenty-first century and its impact on calcifying organisms *Nature* **437** 681–6

- Renault L, Hall A and McWilliams J C 2015 Orographic shaping of US West Coast wind profiles during the upwelling season *Climate Dynamics* (Berlin: Springer) pp 1–17
- Rhein M *et al* 2013 Observations: ocean *Climate Change 2013: The Physical Science Basis. Contribution of Working Group I to the Fifth Assessment Report of the Intergovernmental Panel on Climate Change* ed T F Stocker *et al* (Cambridge: Cambridge University Press) p 62 ([www.ipcc.ch/pdf/assessment-report/ar5/wg1/WG1AR5\\_Chapter03\\_FINAL.pdf](http://www.ipcc.ch/pdf/assessment-report/ar5/wg1/WG1AR5_Chapter03_FINAL.pdf))
- Schwing F B and Mendelssohn R 1997 Increased coastal upwelling in the California current system *J. Geophys. Res.* **102** 3421–38
- Seo H, Brink K H, Dorman C E, Koracin D and Edwards C A 2012 What determines the spatial pattern in summer upwelling trends on the US West coast? *J. Geophys. Res.* **117** C08012
- Shchepetkin A F and McWilliams J C 2005 The regional oceanic modeling system (ROMS): a split-explicit, free-surface, topography-following-coordinate oceanic model *Ocean Modelling* **9** 347–404
- Smith R *et al* 2010 The Parallel Ocean Program (POP) Reference Manual *Technical Report LAUR-10-01853* Los Alamos National Laboratory, Los Alamos, NM, USA ([www.cesm.ucar.edu/models/cesm1.0/pop2/doc/sci/POPRefManual.pdf](http://www.cesm.ucar.edu/models/cesm1.0/pop2/doc/sci/POPRefManual.pdf))
- Snyder M A, Sloan L C, Diffenbaugh N S and Bell J L 2003 Future climate change and upwelling in the California current *Geophys. Res. Lett.* **30** 1823
- Soto C G 2002 The potential impacts of global climate change on marine protected areas *Rev. Fish Biol. Fisheries* **11** 181–95
- Sydeman W J, García-Reyes M, Schoeman D S, Rykaczewski R R, Thompson S A, Black B A and Bograd S J 2014 Climate change and wind intensification in coastal upwelling ecosystems *Science* **345** 77–80
- Takahashi T *et al* 2009 Climatological mean and decadal change in surface ocean pCO<sub>2</sub>, and net sea–air CO<sub>2</sub> flux over the global oceans *Deep-Sea Res. II* **56** 554–77
- Turi G, Lachkar Z and Gruber N 2014 Spatiotemporal variability and drivers of pCO<sub>2</sub> and air–sea CO<sub>2</sub> fluxes in the California Current System: an eddy-resolving modeling study *Biogeosciences* **11** 671–90
- Waldbusser G G, Hales B, Langdon C J, Haley B A, Schrader P, Brunner E L, Gray M W, Miller C A and Gimenez I 2014 Saturation-state sensitivity of marine bivalve larvae to ocean acidification *Nat. Clim. Change* **5** 273–80
- Waldbusser G G, Hales B, Langdon C J, Haley B A, Schrader P, Brunner E L, Gray M W, Miller C A, Gimenez I and Hutchinson G 2015 Ocean acidification has multiple modes of action on *Bivalve* larvae *PLoS One* **10** e0128376
- Waldbusser G G and Salisbury J E 2014 Ocean acidification in the coastal zone from an organism’s perspective: multiple system parameters, frequency domains, and habitats *Annu. Rev. Mar. Sci.* **6** 221–47
- Wang D, Gouhier T C, Menge B A and Ganguly A R 2015 Intensification and spatial homogenization of coastal upwelling under climate change *Nature* **518** 390–4
- Williams N L, Feely R A, Sabine C L, Dickson A G, Swift J H, Talley L D and Russell J L 2015 Quantifying anthropogenic carbon inventory changes in the Pacific sector of the Southern ocean *Mar. Chem.* **174** 147–60
- Wootton J T, Pfister C A and Forester J D 2008 Dynamic patterns and ecological impacts of declining ocean pH in a high-resolution multi-year dataset *Proc. Natl Acad. Sci. USA* **105** 18848–53
- Zeebe R E 2012 History of seawater carbonate chemistry, atmospheric CO<sub>2</sub>, and ocean acidification *Annu. Rev. Earth Planet. Sci.* **40** 141–65
- Zwiers F W and von Storch H 1995 Taking serial correlation into account in tests of the mean *J. Clim.* **8** 336–51